Synthesis and Rheological Characterization of Star-Shaped and Linear Poly(hydroxybutyrate)

3 AUTHORS, INCLUDING:

Savvas G Hatzikiriakos

University of British Columbia - Vancouver

247 PUBLICATIONS   **3,724** CITATIONS

Synthesis and Rheological Characterization of Star-Shaped and Linear Poly(hydroxybutyrate)

Tannaz Ebrahimi,[†,‡] Savvas G. Hatzikiriakos,[*,‡] and Parisa Mehrkhodavandi[*,†]

[†]Department of Chemistry, University of British Columbia, 2036 Main Mall, Vancouver, British Columbia, Canada
[‡]Department of Chemical and Biological Engineering, University of British Columbia, 2360 East Mall, Vancouver, British Columbia, Canada

S *Supporting Information*
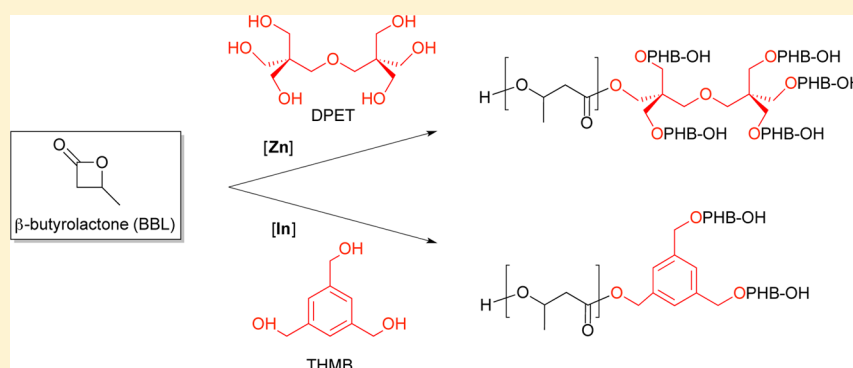
ABSTRACT: Indium and zinc complexes, $[(NNO_{tBu})InCl]_2(\mu\text{-Cl})(\mu\text{-OTHMB})$ (**2**) and $(NN_iO_{tBu})Zn(CH_2CH_3)$ (**3**), were used to produce monodispersed three- and six-armed star-shaped PHBs using tris(hydroxymethyl)benzene (THMB) and dipentaerythritol as the chain transfer agents. Reactions catalyzed by complex **2** were highly controlled, with THMB:catalyst ratios of up to 590:1, resulting in star-shaped PHBs with predictable molecular weights (M_n = 1.25−219 kDa) and narrow dispersities ($Đ$ = 1.02−1.08). The zinc-based catalyst, **3**, was less controlled than the indium analogue but nevertheless generated moderately syndiotactic PHBs with maximum M_n values of ~100 kDa. Importantly, **3** allowed the formation of previously unknown 6-armed star PHBs, allowing us to compare the effects of the different PHB architectures on the rheological behavior of the materials. High molecular weight linear and star polymers were characterized using solution and melt viscoelastic studies. Zero-shear viscosity of linear PHBs exhibited a power law relationship with the span molecular weight; however, it scaled exponentially for star polymers with slightly higher values for the 6-armed star PHBs. This was attributed to the moderately syndiotactic microstructure of these polymers. The absence of a district arm retraction relaxation in the dynamic master curves, and overshoot in the transient viscosity for the 6-armed star PHBs, are due to the lower entanglement density and slightly broader molecular weight distribution of these polymers.

INTRODUCTION

Poly(hydroxybutyrate) (PHB) is a biodegradable and biocompatible polyester with great potential in applications ranging from packaging industries to medicine.[1] Poly(hydroxybutyrate) is produced by microorganisms as intracellular carbon and energy storage granules which can be harvested; however, these fermentation techniques produce highly crystalline PHBs with undesirable processing properties.[2] Alternatively, ring-opening polymerization (ROP) of strained cyclic ester, β-butyrolactone (BBL) with a range of metal-based catalysts,[3] can control polymer macro- and microstructure with various degrees of success.[4] Among these, some are capable of living polymerization and forming PHB with narrow dispersity.[3k,5]

As an alternative to living polymerization, immortal ROP of BBL in the presence of protic groups like alcohols allows the generation of more than one polymer chain per catalyst and can enhance catalyst productivity.[6] Immortal polymerization of

lactide (LA) in the presence of linear and branched alcohols to form linear or branched PLA has been studied in detail.[7] However, similar studies for PHB are rare, in part due to the difficulties inherent in ring-opening polymerization of BBL.[4] Star shaped and highly branched polymers are known for their smaller hydrodynamic radii, lower viscosity, enhanced processability, and increased concentration of functional groups.[7b,8] To date, four-armed star PHBs have been synthesized through ring-opening polymerization of BBL in the presence of ethoxylated pentaerythritols and Sn[9] and Lu[10] based catalysts; however, due to the prevalence of transesterification reactions and lack of catalyst reactivity, the resulting polymers showed broad disparities and/or low molecular weights. Moreover, to

Scheme 1. Complexes 1−3 as Catalysts for the Living and Immortal Ring-Opening Polymerization (ROP) of Lactide (LA) and β-Butyrolactone (BBL)
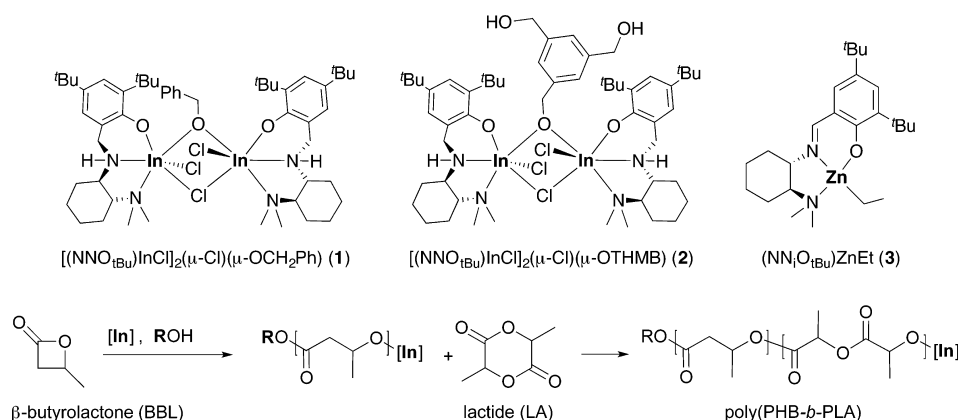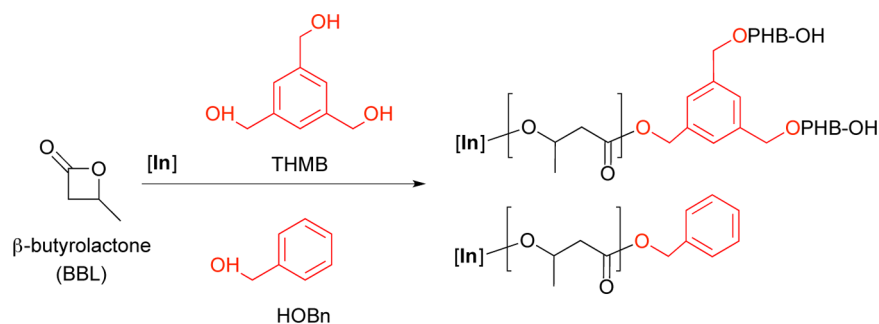

Table 1. Polymerization of BBL in the Presence of BnOH and THMB

entry[a]	ROH	[M]:[ROH]:[I]	conv[b] (%)	$M_{n,theo}$[c] (Da)	$M_{n,GPC}$[d] (Da)	$M_{w,GPC}$[d] (Da)	Đ[d]	T_g (°C)[g]
1	BnOH	5000/190/1	>99	2433	2370[e]	–	–	–[h]
2	BnOH	5000/40/1	>98	10714	12320 (12402[e])	12800	1.04	–[h]
3	BnOH	5000/20/1	>98	21260	22560 (22836[e])	23010	1.02	–[h]
4	BnOH	5000/10/1	>98	42352	48090	49050	1.02	0.5
5	BnOH	5000/5/1	>99	83258	89100	91770	1.03	1.1
6	BnOH	5000/2.7/1	>98	156342	121360	143200	1.17	2.3
7	BnOH	5000/1.66/1	>99	256823	157380	162100	1.03	1.5
8	BnOH	5000/1.25/1	>99	341024	222790	225020	1.03	2.1
9	THMB	7400/590/1	>87	1107	1250[e]	–	–	–[h]
10	THMB	5000/300/1	>97	1560	1695[e]	–	–	–[h]
11[f]	THMB	5000/40/1	>99	10822	9820 (9946[e])	10507	1.07	–[h]
12[f]	THMB	5000/20/1	96	20830	23200 (24010[e])	23660	1.02	–[h]
13	THMB	5000/10/1	95	41061	44490 (46930[e])	44930	1.01	0.5
14	THMB	5000/5/1	>99	85397	77200	83380	1.08	1.0
15	THMB	5000/4/1	>99	106704	111010	116020	1.04	1.5
16	THMB	10000/4/1	>96	206782	138030	146280	1.06	0.5
17	THMB	20000/4/1	>90	387573	219600	223300	1.02	1.5

[a]For entries 1−8, initiator [I] is **1**; for entries 9−17 [I] is **2**. [b]Monomer conversion, determined by ^{1}H NMR spectroscopy. [c]Calculated from $([BBL]_0/([ROH]/[I]) \times$ monomer conversion $\times M_{BBL}) + M_{ROH}$ (M_{BBL} = 86.09 Da, M_{BnOH} = 108.14 Da, M_{THMB} = 168.19 Da). [d]Determined by GPC-LLS using dn/dc = 0.068 for PHB in THF, Đ = dispersity index. [e]^{1}H NMR molecular weight. [f]Reference 13. [g]Determined using DSC. [h]Not determined.

the best of our knowledge there are no in-depth rheological characterization of PHB-containing star polymers.

We have reported that dinuclear indium complex bearing a chiral diamino phenoxy ligand $[(NNO_{tBu})InCl]_2(\mu$-Cl$)(\mu$-OEt$)$ is an active catalyst for the living and immortal ROP of LA[11] and BBL.[12] It is a remarkably active initiator for the highly controlled immortal ROP of BBL in the presence of chain transfer agents such as ethanol and monomethylated poly(ethylene glycol),[12a] allows for copolymerization of lactide and BBL to form controlled A−B−C type triblock polymer by simple sequential addition,[12b] and can be readily converted to other alkoxy-bridged complexes $[(NNO_{tBu})InCl]_2(\mu$-Cl$)(\mu$-OCH$_2$Ph$)$ (**1**) and $[(NNO_{tBu})InCl]_2(\mu$-Cl$)(\mu$-OTHMB$)$ (**2**) ($[OTHMB]^-$ = 3,5-bis(hydroxymethyl)phenyl)methoxide) (Scheme 1).[13] Recently, we reported that complex **2** is the intermediate for formation of star-shaped LA-BBL block copolymers via immortal ROP.[13] We have also reported zinc complexes with the same ligand framework[14] and have expanded work to imine analogues (±) $(NN_iO_{tBu})ZnEt$ (**3**).[15]
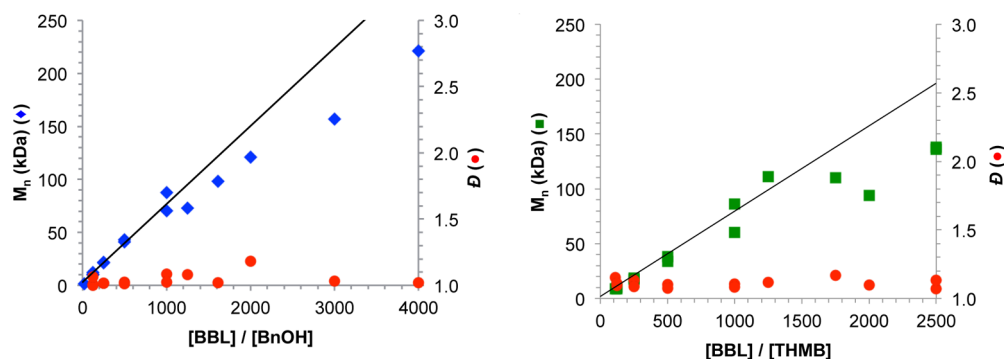
Figure 1. Plots of observed PHB M_n and dispersity (●) as functions [BBL]:[initiator] for (a) left, (◆) BnOH + catalyst **1** and (b) right, (■) THMB + catalyst **2**. The line indicates calculated M_n values based on the BBL:initiator ratio. All reactions were carried out at room temperature in THF, and polymer samples were obtained at >98% conversion.

RESULTS AND DISCUSSION

Immortal ROP of BBL with Complexes 1 and 2 in the Presence of BnOH and THMB. Up to 20 000 equiv of BBL can be polymerized with catalysts **1** and **2** in the presence of high loadings of BnOH and THMB to form linear and star-shaped poly(hydroxybutyrate) (Table 1). The resulting polymers show narrow dispersities ($Đ$ = 1.01–1.08) with good agreement between calculated and experimental molecular weights (Figure 1). In particular, this system forms highly controlled star-shaped polymers in the presence of a wide range of monomers: a THMB:**2** ratio of 590 can be used to generate well-controlled star-shaped oligomers (Table 1, entry 9), while with a ratio of 4:1 star-shaped polymers with molecular weights as high as 220 kDa can be obtained. All PHBs generated with the indium catalysts are atactic.[12a]

Figure 2a shows the ^{1}H NMR spectrum of the oligomers obtained from the polymerization of [BBL]/[THMB]/[**2**] 7400:590:1, which was quenched at 87% conversion and the unreacted monomer removed *in vacuo*. The spectrum shows diagnostic chain end PHB(CH_3)−CH−OH methine protons at 4.2 ppm (peak g) and the core aryl protons at 7.3 ppm (peak a), which confirms the presence of THMB as the polymer core. The integral ratio of the PHB methine protons (peaks e + g) to peak a is ∼4. This value corresponds to the expected number of repeat units per arm of the star (7400/590·0.87/3 = 3.63). These results are also confirmed by the MALDI-TOF mass spectrum (Figure 2b).

Immortal ROP of BBL with Complex 3 in the Presence of Dipentaerythritol (DPET). In order to synthesize multibranched star PHBs, dipentaerythritol (DPET) can be used as the chain transfer agent.[17] However, attempts to prepare star polymers with indium catalysts were unsuccessful; generation of macroinitiators through reacting [(NNO$_{tBu}$)-

InCl]$_2$(μ-Cl)(μ-OEt) with DPET prior to monomer addition failed due to insolubility of DPET in various organic solvents. Polymerization of BBL in the presence of DPET and catalyst at room temperature formed a mixture of linear and star shaped polymers, indicating that the rate of propagation is higher than alcoholysis under these reaction conditions. Reactions at higher temperatures in the presence of catalysts are not controlled. Indeed, the reaction of DPET and neat BBL at 120 °C *without added catalyst* results in uncontrolled BBL polymerization with broad molecular weight distribution, with a side reaction that forms crotonate end groups (Figure S5). We attempted an alkane elimination strategy with indium alkyl[18] complexes; however these proved unreactive under the reaction conditions.

Alternatively, we can use the zinc alkyl complex, **3**, which itself is not a reactive initiator for BBL polymerization in the absence of a nucleophile, to generate high molecular weight star PHBs (Table 2). Ring-opening polymerization of BBL with **3** and DPET forms sydio-rich PHB with P_r values ranging around 0.55−0.62. DSC thermograms of this set of polymers show a broad melting range from 50 to 62 °C with low melting enthalpies of 2.3−3.5 J/g, which shows that the samples are mainly amorphous (Figure S15). The dispersities of the resulting polymers are ∼1.2, and as the monomer-to-catalyst ratio increases, the molecular weight does not increase proportionally due to elimination reactions; the maximum accessible molecular weight using this catalytic system is ∼100 kDa (Figure 3).[5a] Chain end analysis of a representative sample (BBL/DPET/**2**: 294/1/1) using ^{1}H NMR spectroscopy reveals the absence of DPET alcohol resonances at 0.44 and 3.59 ppm and the presence of a broad resonance at 4.14 ppm corresponding to the polyol core, which confirms activation of all six alcohol functionalities for each catalyst (Figure S6). The presence of the DPET core is also confirmed by ^{13}C DEPT and MALDI-TOF results (Figures S7 and S8).

Solution Viscometry. Star-shaped PHB polymers, and their rheology, are unexplored. We studied the solution and melt rheological properties (viscoelasticity) of the synthesized polymers to characterize their topology and bulk properties.

Plots of molecular weight dependence of intrinsic viscosities of linear and star-shaped PHBs are shown in Figure 4. These values are consistent with the results obtained from a Cannon−Fenske viscometer in THF (Figure S20a−d). It is apparent that at a given molecular weight [η] decreases for both sets of star polymers and more significantly for 6-armed star PHBs compared to their linear counterparts. Using the power law Mark−Houwink equation, the following values of the
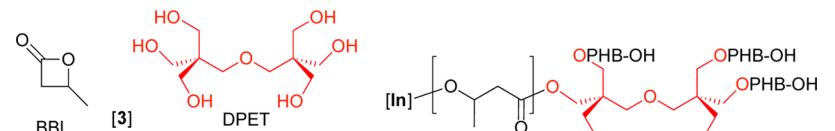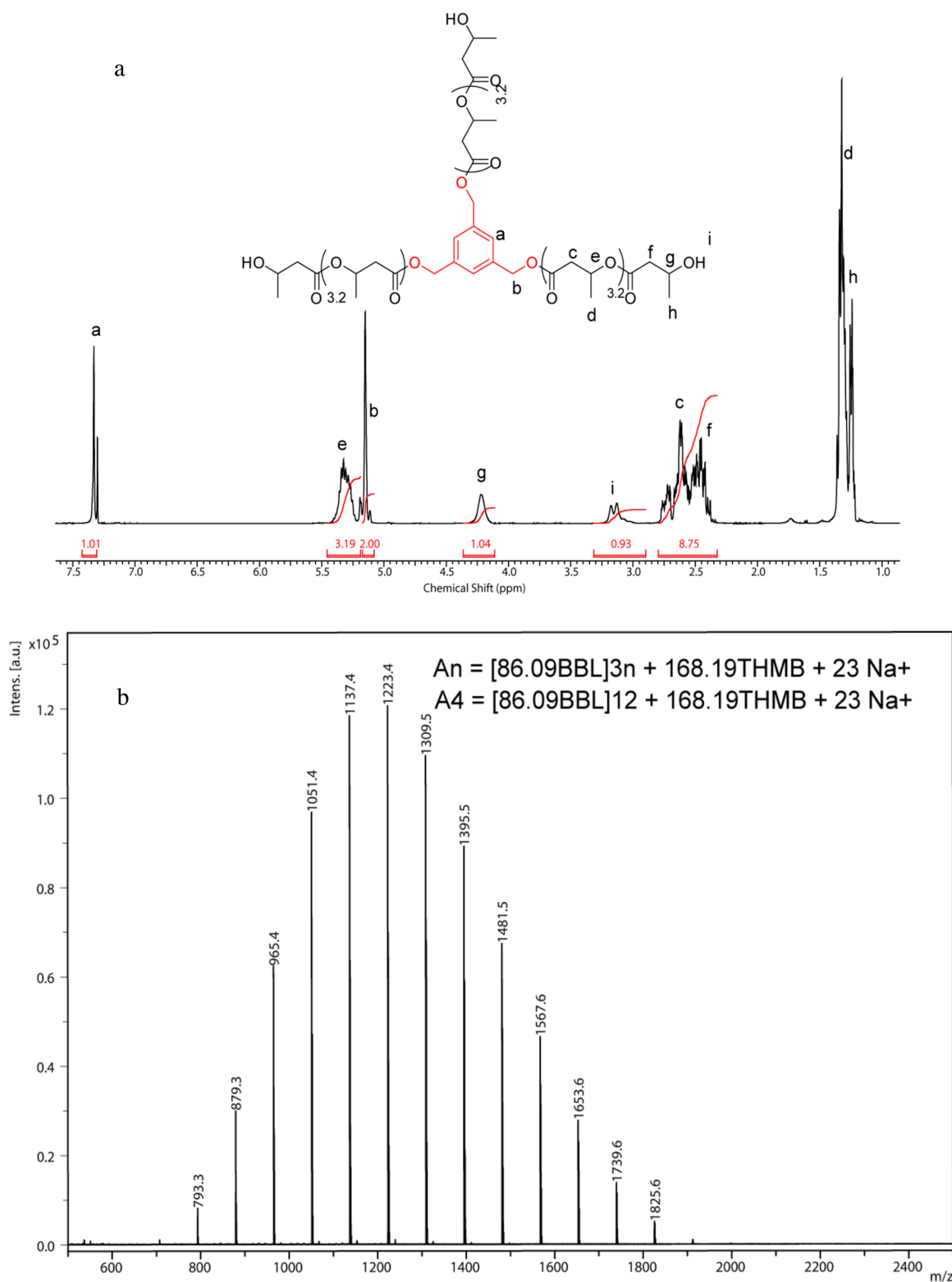
Figure 2. (a, top) ^{1}H NMR spectrum (CDCl$_3$, 25 °C) and (b, bottom) MALDI-TOF spectrum of 3-arm star PHB isolated from polymerization of [BBL]:[THMB]:[1] ratios of 7400:590:1 (Table 1, entry 9). Reaction stopped after 87% conversion, and the monomer leftovers were removed under high vacuum overnight.

parameters were determined for the three classes of PHB polymers: $[\eta]_{\text{linear}} = 0.019 M_{\text{w,LS}}^{0.74}$, $[\eta]_{\text{3-armed-star}} = 0.013 M_{\text{w,LS}}^{0.76}$, $[\eta]_{\text{6-armed-star}} = 0.008 M_{\text{w,LS}}^{0.79}$. The Mark–Houwink exponent is between 0.74 and 0.79. This exponent is 0.5 in poor solvent, such as hexanes, and 0.8 in good solvent,

such as THF, conditions. These results show that THF is a good solvent for linear and branched PHBs and the polymers possess random coil conformation in this solvent.

The measured values of the hydrodynamic radii, R_{h}, the radius of gyration, R_{g}, and their ratio $(R_{\text{g}}/R_{\text{h}})$ are depicted in

Table 2. Polymerization of High Equivalents BBL by Complex 2 in the Presence of DPET[a]

entry	[M]:[ROH]:[I]	conv[b] (%)	$M_{n,theo}$[c] (Da)	$M_{n,GPC}$[d] (Da)	$M_{w,GPC}$[d] (Da)	Đ[d]	P_r[f]	T_g (°C)	T_m (°C)
1	294/1/1	98	25538	26120 (25796[e])	27950	1.07	0.54	—[h]	—[h]
2	670/1/1	89	51589	43190	51390	1.20	0.55	1.2	—[h]
3	822/1/1	88	60358	48200	61700	1.30	0.54	1.5	48.2
4	940/1/1	90	70086	67840	76660	1.13	0.58	0.8	52.1
5	1200/1/1	86	89099	79200	82360	1.04	0.60	0.2	50.9[g]
6	1300/1/1	85	95383	85860	96160	1.12	0.55	2.0	49.3[g]
7	2050/1/1	80	141441	101300	115900	1.14	0.62	2.5	62.3[g]

[a]All reactions were carried out at room temperature in CH_2Cl_2. ROH = DPET, I = complex **3**. [b]Monomer conversion, determined by ^1H NMR spectroscopy. [c]Calculated from $([BBL]_0/([ROH]/[I]) \times$ monomer conversion $\times M_{BBL}) + M_{ROH}$ (M_{BBL} = 86.09 Da, M_{DPET} = 254.28 Da). [d]Đ = dispersity index, determined by GPC-LLS using dn/dc = 0.060 for 6-armed star PHBs in THF. [e]^1H NMR molecular weight (Figure S6). [f]P_r is the probability of racemic linkages between monomer units and is determined by methane region of invers gated $^{13}C\{^1H\}$ NMR spectra (Figures S9–S14). [g]DSC thermograms are presented in Figure S15. [h]Not determined.
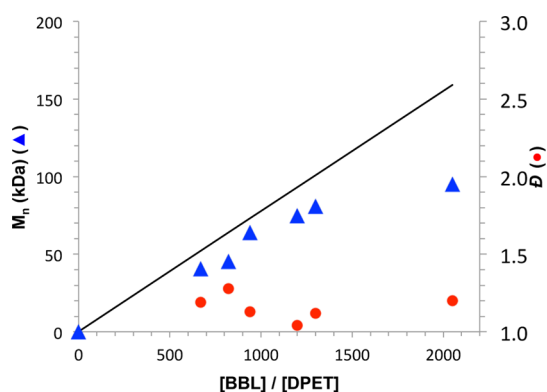

Figure 3. Plots of observed PHB M_n (▲) and dispersity (●) as functions [BBL]:[DPET] for catalyst **3**. The line indicates calculated M_n values based on the (BBL:initiator ratio) × 90%conversion. All reactions were carried out at room temperature in CH_2Cl_2, and polymer samples were obtained at >85% conversion.
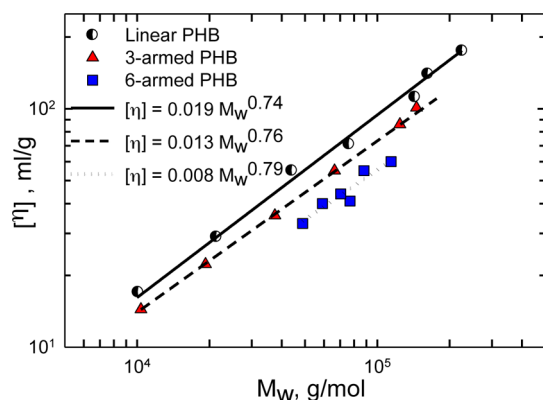

Figure 4. Intrinsic viscosities of PHBs of different architecture versus weight-average molecular weight (M_w) at 25 °C. The slopes of the straight lines (Mark–Houwink exponents) are 0.74 for linear, 0.76 for 3-armed, and 0.79 for 6-armed samples, implying good-solvent conditions.

Figures 5a and 5b for the 3-armed and 6-armed star series as a function of M_w. The power-law relationship of R_h and R_g with M_w of the samples indicated that the molecules are highly self-similar. The compactness factor, R_g/R_h, is 0.78 for a hard sphere, while for a linear polymer chain the value is 1.86. For self-similar structures, the ratio is constant, and as the ratio of R_g/R_h decreases, the intramolecular crowding increases, which indicates enhanced packing of segments within a molecule. For the present materials, the range is very narrow (1.78 < R_g/R_h < 2) for linear PHBs, thereby implying that the molecules are monodispersed; this ratio is 1.35 < R_g/R_h < 1.4 for the 3-armed-PHBs and 1.2 < R_g/R_h < 1.25 for the 6-armed samples. The constant values of the compactness factor and the fact that increasing the branching number reduces the R_g/R_h demonstrate that the branching is structurally well-defined, regular, and compact for both sets of star polymers.

Melt Viscoelastic Properties: Dynamic Frequency Sweep Tests. Figure 6 shows representative master curves of the viscoelastic moduli of linear, 3-armed, and 6-armed star polymers of high molecular weights. The master curves were obtained by superposing the isothermal linear frequency sweep test results of the polymers measured from 25 to 70 °C. The various curves were shifted by means of applying the time–temperature superposition (tTS) principle in order to generate the master curves at the reference temperature of T_{ref} = 50 °C. In order to produce smooth master curves, both horizontal a_T and vertical shift factors b_T, which was close to 1, were used. a_T values versus temperature obey the Arrhenius equation, $a_T = \exp[-E_a/R(1/T - 1/T_r)]$, where E_a is the activation energy of flow, R is the universal gas constant, and T_r is the reference temperature. Straight line fitting of the data results in an average activation energy of 129.1 kJ/mol for the linear, 135.8 kJ/mol for the 3-armed, and 155.4 kJ/mol for 6-armed star PHBs. Increased flow activation energies of the star polymers indicate the influence of the presence of branches on the viscoelastic properties of the polymers. Also using the WLF equation, $\log(a_T) = -C_1(T - T_r)/(C_2 + T - T_r)$, the following parameters were obtained: C_1 = 7.2 K^{-1} and C_2 = 110.1 K for linear polymer and 6.7 K^{-1}, 103.1 K for 3-armed and 7.5 K^{-1}, and 100.8 K for 6-armed samples (Figure S16g). Applicability of the tTS principle and the WLF equation indicated that the samples in the measuring temperature window are all thermorheologically simple fluids.

Similar plots to those depicted in Figure 6 were also prepared for a range of molecular weights of the linear and star polymers
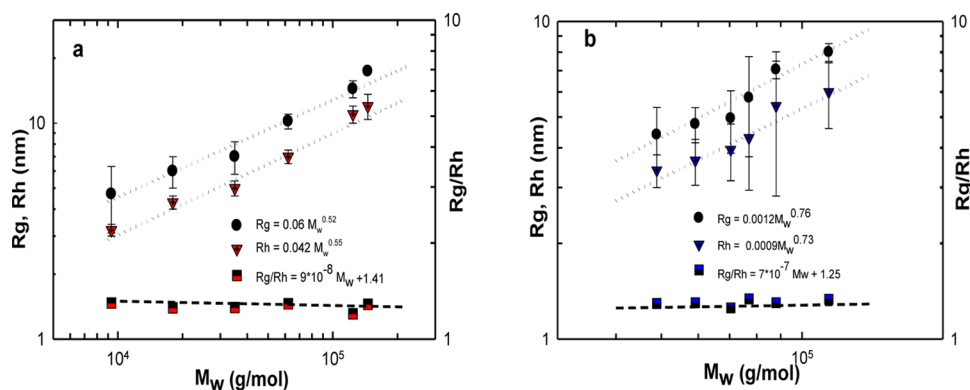
Figure 5. Measured radii of gyrations and hydrodynamic radii vs weight-averaged molecular weight in a series of (a) 3-armed and (b) 6-armed star polymers. The near constant ratio of R_g/R_h implies a high degree of self-similarity in the branching structure of materials.
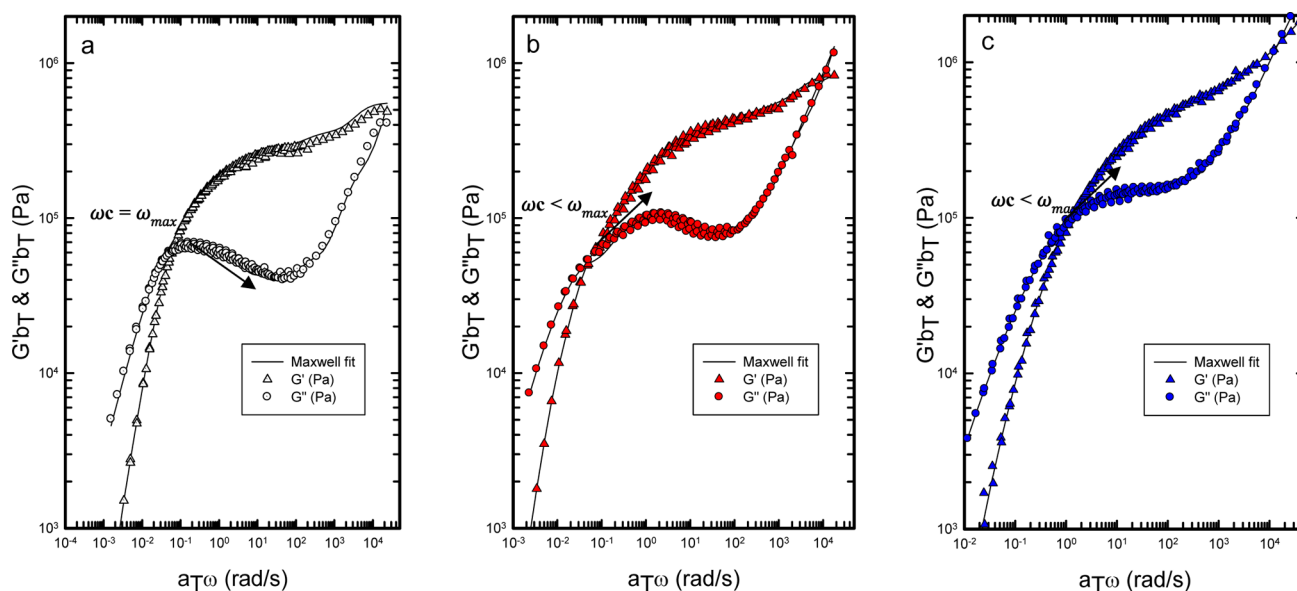

Figure 6. Master curves of the dynamic moduli G' and G'' as a function of angular frequency ω for the PHB melts at 50 °C (a) entry 7 in Table 1 (linear PHB, M_w = 162 kDa, Đ = 1.03), (b) entry 16 in Table 1 (3-armed star PHB, M_w = 146 kDa, Đ = 1.06), and (c) entry 7 in Table 2 (6-armed star PHB, M_w = 115 kDa, Đ = 1.14). Continuous lines represent the fitting of the parsimonious relaxation spectrum (eqs S1 and S2) (molecular weight dependence of G' and G'' of linear, 3-armed, and 6-armed stars are presented in Figure S16a−f).

(Figure S16). All the curves converged at very high frequencies in the transition to the glassy zone. The rubbery region was also clearly observed within the intermediate frequency zone, which is an indicator of the monodispersity of the polymers. Finally, the terminal zone was reached at very low frequencies, where the characteristic slopes $G' \propto \omega^2$ and $G'' \propto \omega$ were obtained.

Comparing the LVE plots of Figure 6, it is apparent that the frequency dependences of the elastic and loss moduli of linear and star PHBs are different. In the case of linear PHBs, the crossover frequency, ω_c ($G' = G''$), in the terminal region coincides with ω_{max}, revealing an isolated band of relaxation times of a narrow molecular weight distributed polymer. Meanwhile, for the star PHB samples, the ω_c values are higher than the corresponding ω_{max}. This is due to the presence of a different relaxation mechanism, the "arm retraction (breathing mode)" relaxation, significantly different from the reptation mechanism of linear polymers.[19] Although the shape of G'' of entry 16 of Table 1 (Figure 6b) follows the characteristic fingerprint of the breathing mode relaxation of the star branched polymers, the G''_{max} of the 6-armed polymers (Figure 6c) is not as significant as that of the 3-armed polymer.

Entanglement molecular weight of the polymers can be estimated using $M_e = \rho_0 RT/G_N^0$, where ρ_0 is the density, R is the gas constant, T is the measurement temperature, and G_N^0 is the plateau modulus.

In order to estimate the plateau modulus, Van Gurp−Palmen plots (loss-angle(δ) vs complex modulus $|G^*|$) were used[20] (Figure S17). The obtained G_N^0 for linear, 3-armed, and six-armed star samples are 0.5, 0.45, and 0.55 MPa, which are in agreement with the results obtained from the parsimonious relaxation spectrum (Figure S18).

The entanglements molecular weight of linear PHBs, M_e, is calculated from the plateau modulus using $M_e = \rho_0 RT/G_N^0$ assuming a density of 0.90 g/cm³ at T = 313 K, which results in M_e = 4684 Da. In order to obtain a precise estimation of the entanglement molecular weight of the stars, the McLeish−Milner equation was used.[21] Based on their theory, there is an exponential relationship between the zero-shear viscosity (η_0) and arms molecular weight (M_{arm}) as $\eta_0 = A \exp(\gamma(M_{arm}/M_e))$, where A is a constant and γ has the universal value of 0.48.[22] The Newtonian zero-shear viscosities were obtained in the low-frequency region using $\lim_{\omega \to 0} G''(\omega)/\omega = \eta_0$. The results are

F

plotted in Figure 7 for linear and star-shaped PHBs versus the molecular weight of the longest linear span in the molecule
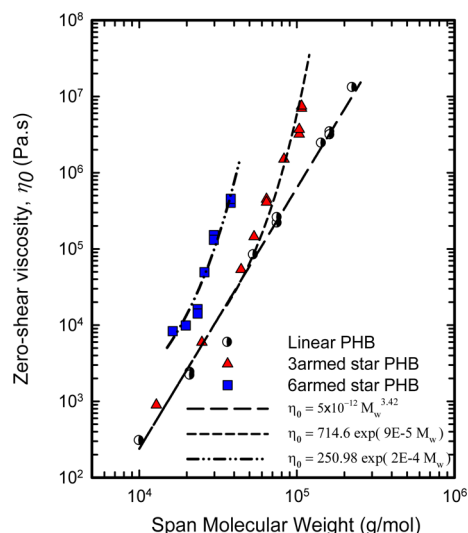

Figure 7. Scaling of the zero shear viscosity on the molecular weight of the series of linear and star-shaped polymers.

(twice the arm molecular weight of a star). The viscosity of the linear polymers follows the power law relationship $\eta_0 = 5 \times 10^{-12} M_w^{3.42}$. Meanwhile, η_0 for symmetric stars scales exponentially with the arm molecular weight.

The exponential dependence of zero-shear viscosity on the molecular weight of star-branched polyisoprenes and other branched polymers such as polyglycerols has been also reported.[19,23] The entanglement molecular weight of the stars estimated from the McLeish−Milner relationship results in M_e value of 5052 and 4800 Da for the 3-armed and the 6-armed star PHBs, respectively. Considering the linear samples as a 2-armed star polymer, for the high molecular weight linear sample examined (entry 7 of Table 1), the branch entanglement number, $Z = M_a/M_e$, is 17, while this number is 9.5 and 4.02 for the 3-armed and the 6-armed star samples shown in Figure 6b,c. Hence, the absence of a distinct arm retraction relaxation mode in the dynamic frequency sweep tests results can be attributed to the lower entanglement density of the 6-armed star PHBs. Additionally the broader molecular weight distribution of this sample (1.14) might be another factor affecting its viscoelastic properties. Nevertheless, arm retraction is still an activated process as it was shown by the exponential dependence of the viscosity of the 6-armed stars on the arm length.

As a universal plot (Figure 7), the zero-shear viscosity versus the span molecular weight should be independent of the number of arms. However, the zero-shear viscosity of 6-arm stars is higher than that of the 3-arms for comparable span molecular weights. Dorgan et al. have also reported the same nonuniversality in zero shear viscosity of the 4-armed and 6-armed star shaped poly(lactic acids), PLAs.[24] They have assigned this lack of universality to several parameters, such as thermal degradation and relatively high molecular weight distributions ($Đ \sim 2$) of the star polymers, which directly affects the symmetry of the star molecules. The rheological measurements of the current work have all been performed at

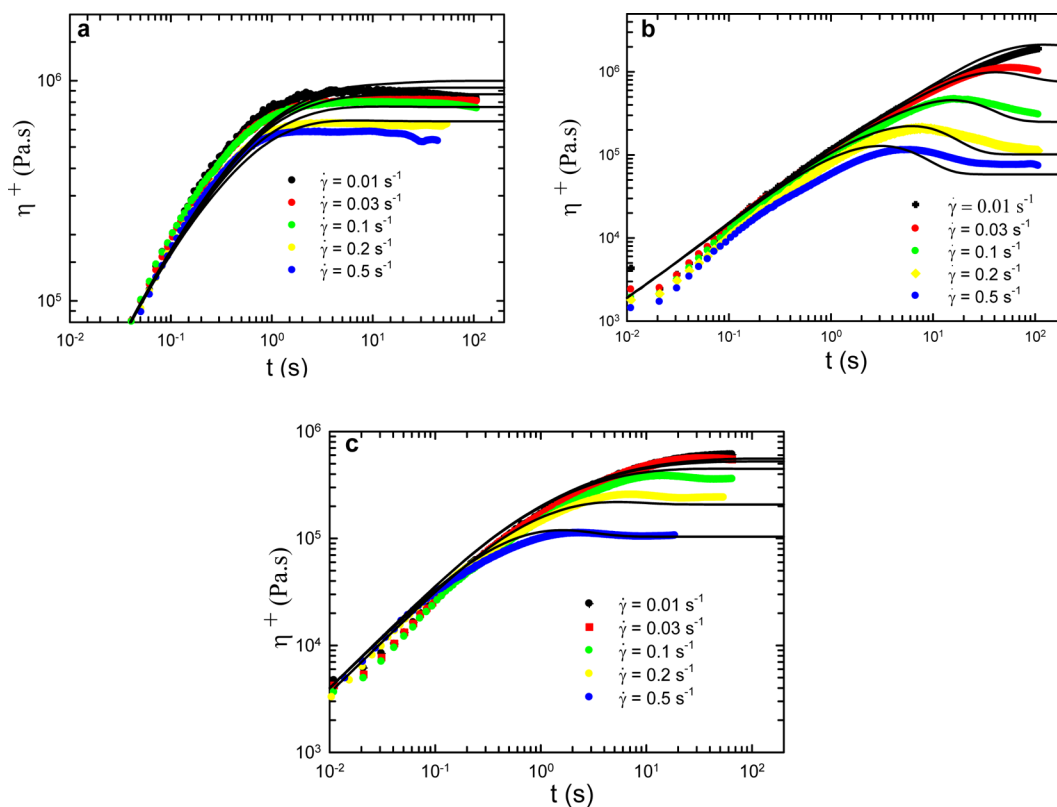**Figure 8.** Shear stress growth coefficient of linear and star-shaped samples at different levels of shear rate, at 50 °C. (a) From Table 1, entry 7 (linear PHB, M_w = 162 kDa, $Đ$ = 1.03). (b) From Table 1, entry 16 (3-armed star PHB, M_w = 146 kDa, $Đ$ = 1.06). (c) From Table 2, entry 7 (6-armed star PHB, M_w = 115 kDa, $Đ$ = 1.14). The continuous lines represent the predictions of the K-BKZ model using Osaki damping functions.

relatively low temperatures, and the dispersities of the polymers are all less than 1.2. Hence, this disparity is attributed to the different chain conformation of moderately syndiotactic microstructure of the 6-armed star PHBs. This observation is consistent with the results reported by Wang et al. on the effect of tacticity on viscoelastic properties of polystyrenes.[25]

Start-Up of Shear Flow Test Results. To examine further the flow properties of PHB melts, startup of steady shear tests was performed at various shear rates to compare the behavior of the various architectures of the PHB polymers (Figure 8). As the shear rate increases, the time-dependent shear growth coefficient reaches an overshoot, followed by a decrease of the steady-state viscosity. The observed viscosity overshoot is likely due to chain alignments,[26] the extent of which is less pronounced for six-armed PHBs, possibly due to its broader molecular weight distribution. Strain hardening due to chain stretching was not observed for the linear and star-shaped PHB samples at the shear rates studied, which is known for monodisperse linear and sparsely branched polymers.

One key observation in Figure 8 is the progressive reduction of transient viscosity with shear rate increase, which is more profound for star-shaped PHBs. This higher degree of shear thinning observed for the stars versus the linear PHBs is consistent with the previously reported results on star-shaped polyisoprenes[23a] and polylactides.[7b,8,24] The lower entanglement density, and the presence of branch tips in the star polymer melts, are the reasons of the observed decreased viscosity at higher shear rates. However, at lower shear rates or in linear viscoelastic region, the branch points enhance the viscosity due to imposing more constraint against molecular movements.

In an attempt to predict the start-up of shear flow results, the Wagner model was used.[16] This model is the simplified version of the K-BKZ as a popular constitutive equation to predict the nonlinear viscoelastic behavior of the polymeric melts, which can be written as follows:

$$\boldsymbol{\sigma} = \int_{-\infty}^{t} \left(\sum_i \frac{gi}{\lambda i} \exp(-(t - t'))/\lambda i \right) h(\gamma) \mathbf{B}(t, t') \, dt' \tag{1}$$

where $\boldsymbol{\sigma}$ and $\mathbf{B}$ are the stress and Finger strain tensors and $h(\gamma)$ represents the damping function. The damping function can be determined using experimental data, if the time-strain separability principle applies to the material. As a result, $h(\gamma) = G(t,\gamma)/G(t)$, which can be determined as a vertical shift factor of the stress relaxation modulus curves, $G(t,\gamma)$ (Figure S19), that best superimpose to the linear relaxation modulus $G(t)$. Data points are finally fitted to the double-exponential Osaki function (eq 2)

$$h(\gamma) = a \exp(-m\gamma) + (1 - a) \exp(-n\gamma) \tag{2}$$

in which a, n, and m are fitting parameters. The Wagner model predictions are shown in Figure 8 as solid lines. The calculated viscosities can satisfactorily predict the viscosity overshoot and more shear thin behavior of the stars compared to the linear PHBs, which shows that the non-Newtonian feature of the star PHBs is predominantly influenced by their relaxation mechanisms under large strains.

CONCLUSIONS

High molecular weight symmetric star-shaped poly-(hydroxybutyrate) were synthesized via immortal ROP of BBL using indium and zinc catalysts in the presence of a triol (THMB) and a hexol (DPET) as the chain transfer agents. The chain end analysis using ^{1}H NMR and MALDI-TOF revealed the presence of the chain transfer agents as the star core. The indium catalyst **2** showed highly controlled living and immortal polymerization of BBL, with each catalyst molecule generating up to 590 macromolecules to afford hydroxyl-functionalized, star-shaped PHBs. Zinc catalyst **3** generates moderately syndiotactic PHBs with maximum molecular weights of ∼100 kDa; however, the presence of side reactions hinders access to higher molecular weights.

The solution and melt viscoelastic properties of the various molecular weight linear and star-shaped PHBs were investigated. Power law relationships of the R_g and R_h with molecular weights and lower amounts of the intrinsic viscosity and compactness factors of the stars compared to that of the linear PHBs indicated the self-similar and symmetric topology of the star PHBs. The entanglement molecular weights of the linear and star-shaped PHB homopolymers were estimated from melt rheology. The zero-shear viscosity of the linear PHBs showed a scaling of $\eta_0 \propto M_w^{3.42}$ to be consistent with those reported for linear monodisperse polymers, while η_0 for symmetric stars scaled exponentially with the arm molecular weight. Furthermore, transient shear viscosity growth of the samples indicates more shear thinning behavior of the stars compared to the linear PHBs due to the dynamic dilution effect of arm tips and lower entanglement densities of the stars, which eases the shear alignment of the chains. We hope to develop our insights into the rheology and synthesis of hydroxyl-functionalized star-shaped PHBs to generate new families of biodegradable materials.

EXPERIMENTAL SECTION

Unless otherwise specified, all the manipulations were performed under an inert atmosphere (N_2) using standard Schlenk, vacuum line, and glovebox techniques. A Bruker Avance 400inv MHz spectrometer and Bruker Avance 400dir MHz spectrometer were used to record the ^{1}H NMR and ^{13}C{^{1}H} NMR. ^{1}H NMR chemical shifts are given in ppm versus residual protons in CDCl$_3$ as δ 7.27. ^{13}C{^{1}H} NMR chemical shifts are given in ppm versus residual ^{13}C in CDCl$_3$ as δ 77.23 ppm. Tetrahydrofuran (THF) was collected from a solvent purification system, further dried over Na/benzophenone and vacuum-transferred to a Strauss flask, and then degassed through a series of freeze–pump–thaw cycles. CDCl$_3$ was dried over CaH$_2$ and vacuum-transferred to a Strauss flask and then degassed through a series of freeze–pump–thaw cycles. Chiral diaminophenolate ligands, H-(NNO$_{tBu}$),[27] dichloride indium complexes, (NNO$_{tBu}$)InCl$_2$,[11a,e,18] and complexes **1, 2**,[13] and **3**[15] were synthesized according to literature procedures.

***In Situ* Preparation of Complex 1 and Representative Large-Scale Immortal Polymerization of BBL with Complex 1 in the Presence of BnOH.** A 20 mL scintillation vial was charged with 1.34 mL of stock solution of [(NNO$_{tBu}$)InCl]$_2$(μ-Cl)(μ-OEt) in THF (0.0027 M, 0.0037 mmol). A 1.5 mL stock solution of BnOH in THF (0.097 M, 0.146 mmol) was added to the catalyst solution and stirred for 1 h and then dried under vacuum for a few hours to remove resulted ethanol and all the solvent and generate complex **1** as a white powder. The white powder, used without further purification, was dissolved in 2 mL of THF, and BBL (1.50 mL, 18.5 mmol) was added dropwise to the stirring solution. The reaction mixture was stirred overnight and then quenched with 0.5 mL of HCl (1.5 M in Et$_2$O). A sample of the mixture was dissolved in wet CDCl$_3$ to be analyzed by ^{1}H NMR spectroscopy to determine conversion. The residue was quenched in cold methanol (0 °C), the precipitated polymer was frozen by immersing the vial in liquid nitrogen, and subsequently the supernatant was decanted off. To remove the trace amounts of the

catalyst, the last three steps were repeated three times, and the isolated polymer was dried under high vacuum for overnight prior to analysis.

***In Situ* Preparation of Complex 2 and Representative Large-Scale Immortal Polymerization of BBL with 2 in the Presence of Tris(hydroxymethyl)benzene (THMB).** In a 20 mL scintillation vial 1.34 mL of stock solution of **1** in THF (0.0027 M, 0.0037 mmol) was added. THMB (25 mg) was dissolved in 2 mL of THF (0.072 M, 0.146 mmol) and added to the catalyst solution, stirred for 1 h, and then dried under vacuum for a few hours to remove resulted ethanol and all the solvent and generate complex **2** as a white powder. The white powder, used without further purification, was dissolved in 2 mL of THF, and BBL (1.50 mL, 18.5 mmol) was added dropwise to the stirring solution. The reaction mixture was stirred overnight and then quenched with 0.5 mL of HCl (1.5 M HCl in Et$_2$O). A sample of the mixture was dissolved in wet CDCl$_3$ to be analyzed by ^{1}H NMR spectroscopy to determine conversion. The residue was quenched in cold methanol (0 °C), and the precipitated polymer was solidified by immersing the vial in liquid nitrogen; subsequently, the supernatant was decanted off. To remove the trace amounts of the catalyst, the last three steps were repeated three times, and the isolated polymer was dried under high vacuum for overnight prior to analysis

Representative Large-Scale Immortal Polymerization of BBL with Complex 3 in the Presence of DPET. In a 20 ml scintillation vial, a slurry of DPET (2.0 mg, 0.0078 mmol) in CH$_2$Cl$_2$ (1 mL) was added to a solution of (NNO$_{tBu}$)Zn(CH$_2$CH$_3$) (**4**) (3.5 mg, 0.0078 mmol) in CH$_2$Cl$_2$ (1 mL) and stirred over 30 min at room temperature prior to the addition of BBL solution (1.3 ml, 16 mmol) in CH$_2$Cl$_2$ (1 mL). The reaction mixture was then stirred for 16 h at room temperature. A sample of the reaction mixture (ca. 0.02 mL) was dissolved in CDCl$_3$ to be analyzed by ^{1}H NMR spectroscopy to determine conversion. The resulting mixture was concentrated under vacuum and quenched by the addition of cold wet methanol. The polymer precipitated from solution and quickly solidified in liquid N$_2$. The supernatant was decanted off, and the polymer was dried under vacuum. To remove the trace amount of the catalyst, the last three steps were repeated three times, and the isolated polymer was dried under high vacuum for overnight prior to analysis.

Solution State Characterization of Polymers. Average molar mass (M_n), dispersity ($Đ$), radius of gyration (R_g), and intrinsic viscosity $[\eta]$ values were determined by a triple detection GPC-LLS-viscometer using an Agilant liquid chromatograph equipped with an Agilant 1200 series pump and autosampler, three Phenogel 5 μm Narrow Bore columns (4.6 × 300 mm with 500 Å, 103 and 104 Å pore size), a Wyatt Optilab differential refractometer, Wyatt miniDAWN TREOS (multiangle laser light scattering detector), and a Wyatt ViscoStar viscometer. The column temperature was 40 °C. A flow rate of 0.5 mL/min was used, and samples were prepared in THF (ca. 1 mg/mL). The refractive index increment dn/dc of each of the three series of the PHB samples (linear, 3-armed, and 6-armed) was measured separately off-line by an Optilab rEX refractive index detector (λ = 658 nm) using a series of different concentration solutions. The operating temperature was 25 °C. Data were processed by ASTRA software (Wyatt Technology).

R_h was measured using a DynaPro-99-E50 dynamic light scattering module with a GaAs laser (658 nm) at 25 °C. The instrument was equipped with a temperature-controlled microsampler (MSXTC-12). Sample concentration was the same as that of the GPC measurements in THF (ca. 1 mg/mL). Intrinsic viscosities of dilute solutions (1−5 mg/mL) of linear and star PHBs were also measured using a Cannon−Fenske viscometer in THF.

MALDI-ToF Characterization of Polymers. Mass spectra were recorded on a Bruker Autoflex MALDI-ToF (time-of-flight mass (ToF) spectrometer equipped with MALDI ion source) operated in either linear or reflection mode. For MALDI-ToF measurement, the sample was dissolved in dichloromethane (0.6 mg/μL); 2,5-dihydroxybenzoic acid (DHB) (0.02 mg/μL) was used as the matrix (10:1), and 1 μL of sodium trifluoroacetate (100 mM) was added as the cation source.

Differential Scanning Calorimeter (DSC). DSC measurements were performed to detect the melting and glass transition temperatures

of the polymers using a TA Instruments Q1000. Experiments were carried out under a nitrogen atmosphere with ~4 mg of the samples sealed in an aluminum pan. After cooling down the samples to the low temperature of −20 °C, they were heated from −20 to 80 °C with a 10 °C/min heating rate, followed by cooling to −20 °C at a 5 °C/min rate, and heated to 80 °C with a 10 °C/min heating rate. The glass transition temperature, T_g, and the melting point, T_m, were determined using the second heating ramp.

Rheological Measurements. All the rheological measurements were performed under a nitrogen atmosphere to minimize degradation of the polymer samples during testing. The linear viscoelastic properties of the samples were determined by a rotational rheometer (Anton-Paar, MCR 501/502) equipped with parallel plate geometry (diameter of 8 mm). Gaps of 0.3−0.6 mm were set to minimize edge effects and ensure a reasonable aspect ratio of plate radius and gap. Dynamic time sweep measurement were carried out at an angular frequency of 1 rad/s and 70 °C for amorphous and semicrystalline samples to examine the thermal stability of the samples. Small-amplitude frequency sweep tests were performed at frequencies in the range of 0.01−100 1/s, with a strain of 1% and temperatures ranging from 25 to 100 °C for amorphous samples and above melting point for the crystalline ones.

Nonlinear tests were performed using a cone and plate geometry with a 25 mm diameter and an angle of 1°. The steady state shear viscosity versus time curves were generated for all samples for shear rates in the range from 0.01 to 0.5 1/s. Also, step shear strain tests were carried out to investigate the relaxation modulus and damping function over a range of strains. The damping functions were used to model the rheological behavior of the samples using the Wagner model.

■ ASSOCIATED CONTENT

Ⓢ Supporting Information

The Supporting Information is available free of charge on the ACS Publications website at DOI: 10.1021/acs.macromol.5b01534.

> ^{1}H NMR and MALDI-ToF analysis of the oligostars; ^{13}C{^{1}H} NMR, GPC traces, and DSC thermograms of the moderately syndiotactic star PHBs; additional dynamic viscoelastic results, calculations, and Mark−Houwink plots of linear, 3-armed, and 6-armed star PHBs plotted using data from the Cannon−Fenske viscometer (PDF)

■ AUTHOR INFORMATION

Corresponding Authors
*E-mail savvas.hatzi@ubc.ca (S.G.H.).
*E-mail mehr@chem.ubc.ca (P.M.).

Notes
The authors declare no competing financial interest.

■ REFERENCES

(1) (a) Ackermann, J.-U.; Müller, S.; Lösche, A.; Bley, T.; Babel, W. *J. Biotechnol.* **1995**, 39 (1), 9−20. (b) Muller, H. M.; Seebach, D. *Angew. Chem., Int. Ed. Engl.* **1993**, 32 (4), 477−502. (c) Chen, G. Q. *Chem. Soc. Rev.* **2009**, 38 (8), 2434−2446.

(2) Kabasci, S. *Bio-Based Plastics: Materials and Applications*; John Wiley & Sons, Ltd.: New York, 2013.

(3) (a) Zintl, M.; Molnar, F.; Urban, T.; Bernhart, V.; Preishuber-Pfugl, P.; Rieger, B. *Angew. Chem., Int. Ed.* **2008**, 47 (18), 3458−3460. (b) Hori, Y.; Takahashi, Y.; Yamaguchi, A.; Nishishita, T. *Macro-*

molecules **1993**, *26* (16), 4388−4390. (c) Kemnitzer, J. E.; McCarthy, S. P.; Gross, R. A. *Macromolecules* **1993**, *26* (23), 6143−6150. (d) Kricheldorf, H. R.; Eggerstedt, S. *Macromolecules* **1997**, *30* (19), 5693−5697. (e) Kricheldorf, H. R.; Lee, S.-R.; Scharnagl, N. *Macromolecules* **1994**, *27* (12), 3139−3146. (f) Guillaume, C.; Carpentier, J. F.; Guillaume, S. M. *Polymer* **2009**, *50* (25), 5909−5917. (g) Ajellal, N.; Bouyahyi, M.; Amgoune, A.; Thomas, C. M.; Bondon, A.; Pillin, I.; Grohens, Y.; Carpentier, J. F. *Macromolecules* **2009**, *42* (4), 987−993. (h) Ajellal, N.; Thomas, C. M.; Carpentier, J. F. *J. Polym. Sci., Part A: Polym. Chem.* **2009**, *47* (12), 3177−3189. (i) Ajellal, N.; Durieux, G.; Delevoye, L.; Tricot, G.; Dujardin, C.; Thomas, C. M.; Gauvin, R. M. *Chem. Commun.* **2010**, *46* (7), 1032−1034. (j) Jaffredo, C. G.; Carpentier, J.-F.; Guillaume, S. M. *Macromolecules* **2013**, *46* (17), 6765−6776. (k) Jaffredo, C. G.; Chapurina, Y.; Guillaume, S. M.; Carpentier, J. F. *Angew. Chem., Int. Ed.* **2014**, *53* (10), 2687−2691. (l) Kramer, J. W.; Coates, G. W. *Tetrahedron* **2008**, *64* (29), 6973−6978.

(4) Carpentier, J. F. *Macromol. Rapid Commun.* **2010**, *31* (19), 1696−1705.

(5) (a) Rieth, L. R.; Moore, D. R.; Lobkovsky, E. B.; Coates, G. W. *J. Am. Chem. Soc.* **2002**, *124* (51), 15239−15248. (b) Amgoune, A.; Thomas, C. M.; Ilinca, S.; Roisnel, T.; Carpentier, J. F. *Angew. Chem., Int. Ed.* **2006**, *45* (17), 2782−2784. (c) Ajellal, N.; Lyubov, D. M.; Sinenkov, M. A.; Fukin, G. K.; Cherkasov, A. V.; Thomas, C. M.; Carpentier, J. F.; Trifonov, A. A. *Chem. - Eur. J.* **2008**, *14* (18), 5440−5448. (d) Kramer, J. W.; Treitler, D. S.; Dunn, E. W.; Castro, P. M.; Roisnel, T.; Thomas, C. M.; Coates, G. W. *J. Am. Chem. Soc.* **2009**, *131* (44), 16042−16044. (e) Bouyahyi, M.; Ajellal, N.; Kirillov, E.; Thomas, C. M.; Carpentier, J. F. *Chem. - Eur. J.* **2011**, *17* (6), 1872−1883.

(6) (a) Amgoune, A.; Thomas, C. M.; Carpentier, J. F. *Macromol. Rapid Commun.* **2007**, *28* (6), 693−697. (b) Chapurina, Y.; Klitzke, J.; Casagrande, O. L.; Awada, M.; Dorcet, V.; Kirillov, E.; Carpentier, J.-F. *Dalton Trans.* **2014**, *43* (38), 14322−14333.

(7) (a) Wang, Y.; Zhao, W.; Liu, X.; Cui, D.; Chen, E. Y. X. *Macromolecules* **2012**, *45* (17), 6957−6965. (b) Corneillie, S.; Smet, M. *Polym. Chem.* **2015**, *6* (6), 850−867. (c) Amgoune, A.; Thomas, C. M.; Carpentier, J. F. *Pure Appl. Chem.* **2007**, *79* (11), 2013−2030. (d) Clark, L.; Cushion, M. G.; Dyer, H. E.; Schwarz, A. D.; Duchateau, R.; Mountford, P. *Chem. Commun.* **2010**, *46* (2), 273−275. (e) Cross, E. D.; Allan, L. E. N.; Decken, A.; Shaver, M. P. *J. Polym. Sci., Part A: Polym. Chem.* **2013**, *51* (5), 1137−1146. (f) Holmberg, A. L.; Reno, K. H.; Wool, R. P.; Epps, T. H. *Soft Matter* **2014**, *10* (38), 7405−7424. (g) Oh, J. K. *Soft Matter* **2011**, *7* (11), 5096−5108.

(8) Kim, E. S.; Kim, B. C.; Kim, S. H. *J. Polym. Sci., Part B: Polym. Phys.* **2004**, *42* (6), 939−946.

(9) Kricheldorf, H. R.; Fechner, B. *J. Polym. Sci., Part A: Polym. Chem.* **2002**, *40* (8), 1047−1057.

(10) Zhao, W.; Li, C. Y.; Liu, B.; Wang, X.; Li, P.; Wang, Y.; Wu, C. J.; Yao, C. G.; Tang, T.; Liu, X. L.; Cui, D. M. *Macromolecules* **2014**, *47* (16), 5586−5594.

(11) (a) Douglas, A. F.; Patrick, B. O.; Mehrkhodavandi, P. *Angew. Chem., Int. Ed.* **2008**, *47* (12), 2290−2293. (b) Othman, N.; Acosta-Ramirez, A.; Mehrkhodavandi, P.; Dorgan, J. R.; Hatzikiriakos, S. G. *J. Rheol.* **2011**, *55* (5), 987−1005. (c) Osten, K. M.; Yu, I.; Duffy, I. R.; Lagaditis, P. O.; Yu, J. C. C.; Wallis, C. J.; Mehrkhodavandi, P. *Dalton Trans.* **2012**, *41* (26), 8123−8134. (d) Othman, N.; Xu, C.; Mehrkhodavandi, P.; Hatzikiriakos, S. G. *Polymer* **2012**, *53* (12), 2442−2452. (e) Yu, I.; Acosta-Ramirez, A.; Mehrkhodavandi, P. *J. Am. Chem. Soc.* **2012**, *134* (30), 12758−12773. (f) Fang, J.; Yu, I.; Mehrkhodavandi, P.; Maron, L. *Organometallics* **2013**, *32*, 6950−6956. (g) Osten, K. M.; Aluthge, D. C.; Patrick, B. O.; Mehrkhodavandi, P. *Inorg. Chem.* **2014**, *53* (18), 9897−9906. (h) Osten, K. M.; Aluthge, D. C.; Mehrkhodavandi, P. *Dalton Trans.* **2015**, *44*, 6126−6139.

(12) (a) Xu, C.; Yu, I.; Mehrkhodavandi, P. *Chem. Commun.* **2012**, *48* (54), 6806−6808. (b) Aluthge, D. C.; Xu, C. L.; Othman, N.; Noroozi, N.; Hatzikiriakos, S. G.; Mehrkhodavandi, P. *Macromolecules* **2013**, *46* (10), 3965−3974.

(13) Yu, I.; Ebrahimi, T.; Hatzikiriakos, S. G.; Mehrkhodavandi, P. *Dalton Trans.* **2015**, *44*, 14248−14254.

(14) Labourdette, G.; Lee, D. J.; Patrick, B. O.; Ezhova, M. B.; Mehrkhodavandi, P. *Organometallics* **2009**, *28* (5), 1309−1319.

(15) Mamleeva, E. M.Sc. Thesis, UBC, 2015.

(16) Dealy, J. M.; Wissbrun, K. F. *Melt Rheology and Its Role in Plastics Processing*, 2nd ed.; Van Nostrand Reinhold: New York, 1990.

(17) Shaver, M. P.; Cameron, D. J. A. *Biomacromolecules* **2010**, *11* (12), 3673−3679.

(18) Acosta-Ramirez, A.; Douglas, A. F.; Yu, I.; Patrick, B. O.; Diaconescu, P. L.; Mehrkhodavandi, P. *Inorg. Chem.* **2010**, *49* (12), 5444−5452.

(19) Fetters, L. J.; Kiss, A. D.; Pearson, D. S.; Quack, G. F.; Vitus, F. J. *Macromolecules* **1993**, *26* (4), 647−654.

(20) Trinkle, S.; Friedrich, C. *Rheol. Acta* **2001**, *40* (4), 322−328.

(21) Milner, S. T.; McLeish, T. C. B. *Macromolecules* **1997**, *30* (7), 2159−2166.

(22) Vega, D. A.; Sebastian, J. M.; Russel, W. B.; Register, R. A. *Macromolecules* **2002**, *35* (1), 169−177.

(23) (a) Das, C.; Inkson, N. J.; Read, D. J.; Kelmanson, M. A.; McLeish, T. C. B. *J. Rheol.* **2006**, *50* (2), 207−234. (b) Kainthan, R. K.; Muliawan, E. B.; Hatzikiriakos, S. G.; Brooks, D. E. *Macromolecules* **2006**, *39* (22), 7708−7717.

(24) Dorgan, J. R.; Williams, J. S.; Lewis, D. N. *J. Rheol.* **1999**, *43*, 1141−1155.

(25) Huang, C.-L.; Chen, Y.-C.; Hsiao, T.-J.; Tsai, J.-C.; Wang, C. *Macromolecules* **2011**, *44* (15), 6155−6161.

(26) (a) Koga, T.; Tanaka, F.; Kaneda, I.; Winnik, F. M. *Langmuir* **2009**, *25* (15), 8626−8638. (b) Snijkers, F.; Ratkanthwar, K.; Vlassopoulos, D.; Hadjichristidis, N. *Macromolecules* **2013**, *46* (14), 5702−5713.

(27) Mitchell, J. M.; Finney, N. S. *Tetrahedron Lett.* **2000**, *41* (44), 8431−8434.